Ultra-Compact Terabit Plasmonic Modulator Array

Ueli Koch, Andreas Messner, Claudia Hoessbacher, Wolfgang Heni, Arne Josten, Benedikt Baeuerle, Masafumi Ayata, Yuriy Fedoryshyn, Delwin L. Elder, Larry R. Dalton, *Senior Member, IEEE, Fellow, OSA*, and Juerg Leuthold, *Fellow, IEEE, Fellow, OSA*

(Invited Paper)

***Abstract*—A new plasmonic transmitter solution offering 0.8 Tbit/s on an ultra-compact 90 μm × 5.5 μm footprint is introduced. It comprises a densely arranged four-channel plasmonic phase modulator array that directly interconnects an optical fiber array. Each plasmonic modulator features high-index grating couplers—for direct and efficient conversion from a fiber mode to a plasmonic slot mode and vice versa—and a plasmonic waveguide—for efficient high-speed modulation. The individual devices achieve data rates of 200 Gbit/s with a symbol rate of 100 GBd. Electrical and optical crosstalk between neighboring modulators were found to have no significant influence on the data modulation experiment. The modulator array has been tested in a 100 GBd experiment with signals at a single wavelength (mimicking a space division multiplexing scheme) and at different wavelengths (mimicking a wavelength division multiplexing experiment).**

***Index Terms*—Electrooptic modulator, nanophotonics, nonlinear optical devices, optical arrays, plasmonics.**

I. Introduction

FUTURE optical interconnect technologies need transceivers with a high level of parallelism on an ultra-small footprint, which offer highest bandwidths at lowest possible power consumption [1]–[6]. Such interconnects are of interest for high performance computing, inter- and intra-data center connections and even for larger communications networks [6]–[9].

Currently, strong efforts are taken to develop a technology that would enable highly parallelized interconnects [3], [4]. Here, research primarily focuses on making compact transmitter arrays, highly parallel transport media and multi-channel receivers available. Among these components, current receiver solutions are already offering high bandwidth and a compact footprint [10]–[16]. Highly parallelized photodetector arrays [17] demonstrate that receiver components are matching interconnect requirements. At the same time, new transport media emerged including fiber arrays [18], multicore [19]–[21] and multimode fibers [22]–[25], which already offer highest densities and transmission capabilities. When it comes to transmitters, the community has already developed attractive solutions based on vertical-cavity surface-emitting lasers (VCSELs). VCSELs are respected as compact components – on-chip interconnect solution [26], PAM8 data modulation [27] and parallelization with 39 μm pitched multicore fibers [28], [29] have already been convincingly demonstrated. Just recently, 700 Gbit/s data modulation have been demonstrated with a VCSEL array coupled to a 7-core multicore fiber [30]. However, overcoming the inherent bandwidth limitations is challenging with the VCSEL technology. Alternatively, external modulators offer higher speed and better signal quality than directly modulated sources. Highest modulation bandwidths can be achieved with external modulators based on $LiNbO_3$ photonics [31]–[33], InP photonics [34]–[42], Si photonics [43]–[47] or plasmonics [48]–[52]. However, dense integration of external modulators based on photonic solutions is challenging due to a large footprint. To reduce the footprint of photonic solutions one may resort to resonant modulators. For instance, ring modulators have already shown remarkably compact footprints down to 6 μm × 5 μm in photonics [53]. However, photonic ring mod-

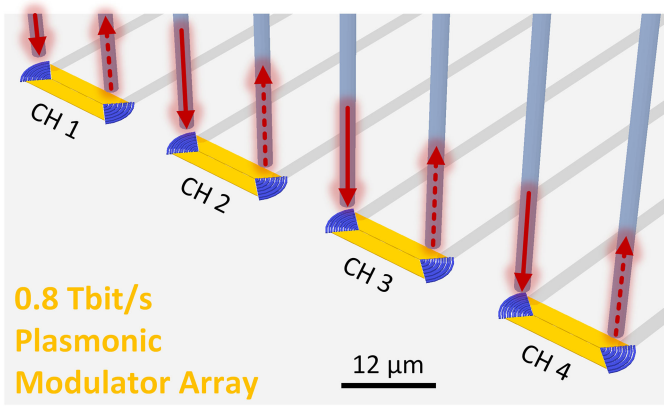

Fig. 1. 3-dimensional rendering of the 4-channel plasmonic modulator array. Each channel is composed of an input coupler, a 9 μm plasmonic phase modulator and an output coupler. The full array is ultra-compact, directly interfaces the 12 μm pitch fiber cores and modulates 4 × 200 Gbit/s.

Manuscript received November 26, 2018; revised February 1, 2019; accepted February 6, 2019. Date of publication February 14, 2019; date of current version March 27, 2019. This work was supported in part by the EU-project PLASMOfab (688166) and in part by ERC grant Plasilor (670478). *(Corresponding author: Ueli Koch.)*

U. Koch, A. Messner, C. Hoessbacher, W. Heni, A. Josten, B. Baeuerle, M. Ayata, Y. Fedoryshyn, and J. Leuthold are with the Institute of Electromagnetic Fields, ETH Zurich, Zurich 8092, Switzerland (e-mail: uelikoch@ethz.ch; amessner@ethz.ch; choessbacher@ethz.ch; wheni@ethz.ch; ajosten@ethz.ch; bbaeuerle@ethz.ch; mayata@ethz.ch; yuriy@ief.ee.ethz.ch; leuthold@ethz.ch).

D. L. Elder and L. R. Dalton are with the Department of Chemistry, University of Washington, Seattle, WA 98195-1700 USA (e-mail: elderdl@uw.edu; dalton@chem.washington.edu).

Color versions of one or more of the figures in this paper are available online at http://ieeexplore.ieee.org.

Digital Object Identifier 10.1109/JLT.2019.2899372

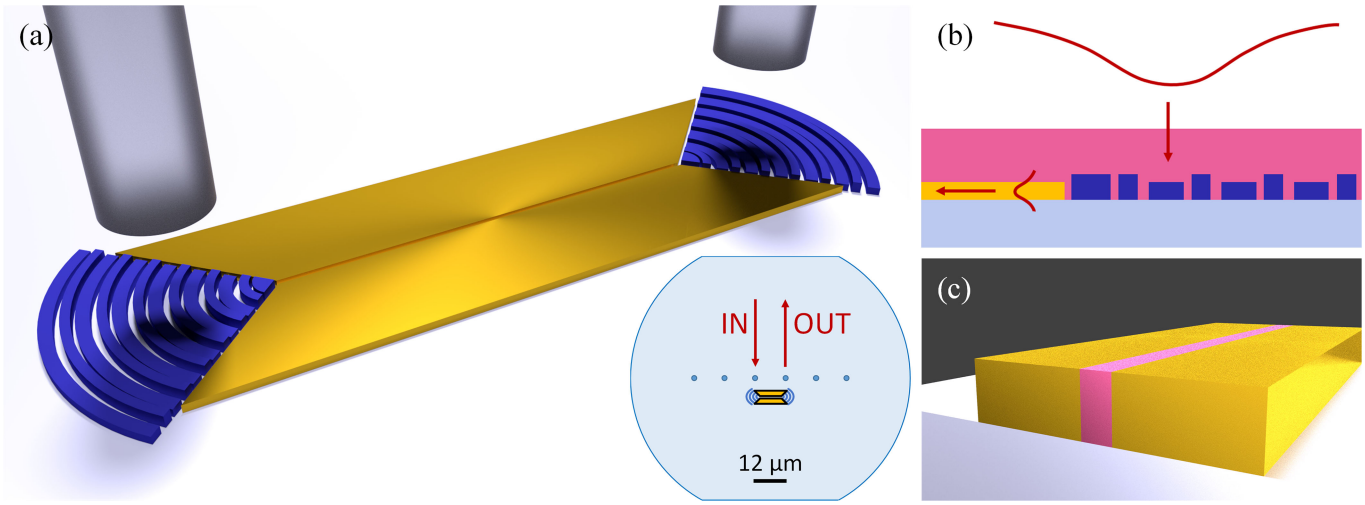

Fig. 2. Plasmonic phase modulator concept for a single device. (a) 3-dimensional rendering of the plasmonic phase modulator consisting of high-index silicon grating couplers (dark blue), a gold plasmonic slot waveguide (gold) and the cores of an optical fiber array (grey). The inset shows the facet of the fiber array. Neighboring cores with a 12 µm pitch were used to couple light into and out of the modulator. (b) Cross-section along the device showing the grating coupler geometry and schematic of the vertically incident fiber mode that is converted to a horizontally propagating plasmonic mode. (c) Cross-section across the plasmonic slot waveguide which is filled by a nonlinear organic electro-optic material (purple). In this configuration, light and electrical signal are both confined to the plasmonic slot leading to strong field enhancement, high field overlap and therefore strongest light-matter interaction.

ulators are limited in bandwidth due to their resonant nature. Plasmonic ring resonators offer a higher bandwidth alternative and smallest modulator footprint [54]. Still, highest bandwidth and best signal quality is achieved in non-resonant plasmonic modulators [52], [55]. They feature an electro-optical bandwidth above 500 GHz [56] and show an electro-optical response until 1.25 THz [57]. Also, a plasmonic modulator array with 4×36 Gbit/s has already been shown [58]. However, although the plasmonic modulators are very small, these modulators end up with a large footprint because of the large dimensions of the photonic couplers and waveguides. A new solution offering a most compact footprint with the advantages of the large bandwidth of an external optical modulator would therefore be of highest interest in view of future ultra-dense parallelized interconnects. Recently, high-speed all-metallic Mach-Zehnder and IQ modulators were introduced [59], [60]. These devices feature a short length of 36 µm to modulate and transmit 116 Gbit/s and 200 Gbit/s, respectively. For higher integration density, even further reduction in footprint would be preferred.

In this paper, we introduce and demonstrate a new plasmonic modulator array concept. The plasmonic modulators feature a short length of 17 µm including the built-in modulation section and novel grating couplers that directly perform fiber-to-plasmonic conversion. This way, unnecessary losses from photonic components and photonic-to-plasmonic converters are avoided. Each modulator is operated at 200 Gbit/s. As the array is composed of four modulators, this results in a total data modulation of 0.8 Tbit/s. The modulators are directly connected through a 12 µm pitched optical fiber array resulting in a record small footprint of 90 µm $\times$ 5.5 µm.

The manuscript is structured as follows: In the first section, the array concept and the working principle of a single channel are introduced. In the following, the implementation of the array is discussed including fabrication and optical and electrical arrangement. Next, the devices are characterized in terms of fiber-to-fiber transmission, frequency response and crosstalk. Both electrical and optical crosstalk between the modulators are investigated and no signficant impairment for parallel array operation is found. Then, high-speed data modulation of each individual channel is shown and high uniformity of the performance of all four modulators is demonstrated. Finally, array operation in different application scenarios is demonstrated at almost single device performance.

The paper is in part based on material first published at the postdeadline session of the 2018 Europen Conference on Optical Communication (ECOC) [61].

II. Concept

The plasmonic array interconnect is composed of four densely arranged compact, high-speed modulator channels, see Fig. 1. The device pitch of only 24 µm allows for the densest arrangement of high-speed data channels, limited only by current fiber array technology. This leads to a record-low footprint of 90 µm $\times$ 5.5 µm to achieve 0.8 Tbit/s data modulation.

A single modulator occupies an area of only 17 µm $\times$ 5.5 µm, including the active plasmonic section of 9 µm length and the fiber-to-chip grating couplers (GCs), see Fig. 2(a). The grating couplers access an optical fiber array (OFA) with 12 µm pitch and 2 µm mode field diameter.

The fiber-to-chip couplers were implemented as high-index silicon GCs. They convert the perpendicularly incident fiber mode directly into a strongly confined on-chip plasmonic slot mode – omitting intermediate guiding in photonic structures, c.f. Fig. 2(b). Such a design advantageously combines photonics and plasmonics, making photonic waveguides and photonic-plasmonic converters obsolete and hence minimizing the insertion loss. The only 9 µm short plasmonic section provides efficient high-speed modulation due to confinement of both optical and electrical fields into the plasmonic slot.

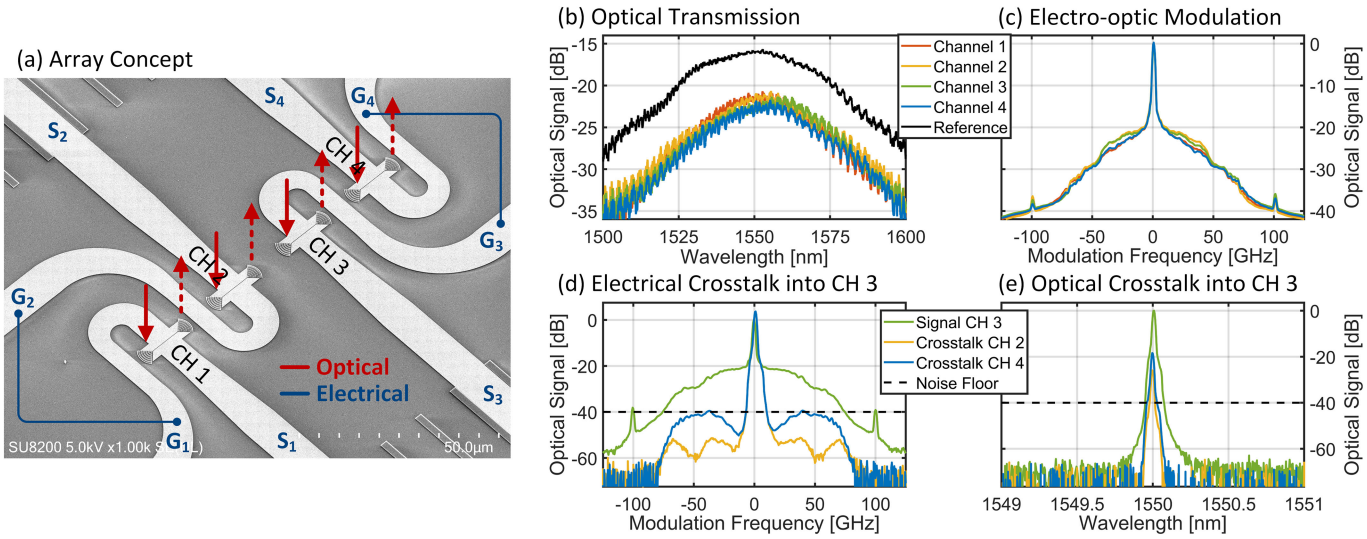

Fig. 3. Array concept, optical transmission, electro-optic modulation and electrical and optical crosstalk measurements. (a) SEM image of the modulator array and arrangement of the parallel plasmonic modulators with the ground-signal contacts. Optical carriers (solid red) are coupled in by every second fiber core and the modulated light (dashed red) is coupled out through the remaining cores. The electrical signal (blue) is applied to the modulators by a multi-channel RF probe. The individual signal lines for channels 1–4 and the corresponding ground lines are marked by S_i and G_i, respectively. (b) Optical transmission spectra of the four plasmonic modulator array channels in comparison to single device transmission. For the array, fiber-to-fiber losses were found to be between 21 dB and 22 dB for an optical carrier at 1550 nm. (c) Electro-optic modulation in the four array channels. The optical carrier was modulated with a 100 GBd non-return-to-zero binary phase shift keying signal and measured in an optical spectrum analyzer in the receiver. (d) Electrical crosstalk measurement performed on channel 3 by measuring the optical transmission spectrum after electro-optic modulation caused by driving adjacent channels. The green line shows the optical spectrum when an electrical signal is applied to channel 3. The yellow and blue lines show the electrical crosstalk of the adjacent channels 2 and 4 into channel 3 – when the latter is switched off. The crosstalk is below the ASE noise floor of a low-noise EDFA (dashed line). (e) Optical crosstalk of −26.0 dB and −18.4 dB from channel 2 and 4, respectively. The optical crosstalk leads to a 1.1 dB electrical SNR penalty extracted from the SDM data experiment described below.

III. Implementation

For the realization of the plasmonic modulator array, nano-scale fabrication as well as optical and electronic routing are crucial for optimal device performance.

The arrays have been fabricated with in-house cleanroom technology. The photonic GCs were defined by fully etching into a 220 nm silicon-on-insulator (SOI) substrate. A grating period of 590 nm was chosen to match the center wavelength to 1550 nm. A two-block design was chosen to reduce back-reflection into the plasmonic slot and to improve mode matching to the fiber mode. The block widths are 238 nm and 173 nm and the block spaces are 59 nm and 120 nm, c.f. Fig. 2(b). A second partial etch of 70 nm was performed to break the symmetry and to improve the coupling efficiency for 90° vertical incidences. The metal slot waveguides of 55 nm width and the electrical routing were fabricated using a gold lift-off process. Finally, the nonlinear organic electro-optic material HD-BB-OH/YLD124 [62] was spin-coated onto the sample to fill the plasmonic slot as depicted in Fig. 2(c). Such processed devices achieve 90° phase modulation in the 11 µm long plasmonic section with a voltage swing of 4 V – extracted from V_{rms} in the 100 GBd BPSK experiment. In this technology, stable operation for more than 11 hours at temperatures up to 75 °C was recently demonstrated [52].

For this first demonstration, plasmonic phase modulators rather than amplitude modulating Mach-Zehnder configurations were chosen to demonstrate the integration concept. Although phase modulators require advanced coherent detection in the receiver, they benefit from a simple transmitter design. Further, phase modulators operate linearly and independently from wavelength and do not require offset voltage biases. This softens the requirements on nano-scale fabrication, improving both yield and uniformity across the devices.

The arrangement of the plasmonic modulators, its electrical lines and optical ports are crucial for best device performance and to understand the origins of potential optical and electrical crosstalk. The scanning electron microscope (SEM) image in Fig. 3(a) shows the device structure. The four channels (CH 1–4) are spaced by 24 µm along a straight line. The optical carrier (solid red) is coupled in via every second GC and the modulated light (dashed red) is coupled out on the neighboring GC after the active plasmonic section. The electrical lines (blue) are labelled with S_i for signal line i and G_i for ground line i of the channel $i = 1$–4, respectively. The ground lines G_2 and G_3 inevitably have to pass between two modulators as no RF line crossings were implementable. Since the modulators have to be poled simultaneously, the ground lines G_1 and G_2 as well as G_3 and G_4 are connected. The poling field was then applied from signal lines S_1 and S_3 to signal lines S_2 and S_4. Subsequently, channel 3 (CH 3) is chosen as a representative channel for worst-case estimations as it sits between two neighboring devices.

IV. Characterization

The device characteristics in terms of fiber-to-fiber transmission, frequency response, and optical and electrical crosstalk

were investigated before performing the data transmission experiment.

A. Fiber-to-Fiber Transmission

Optical fiber-to-fiber losses of 15 dB were found for single devices. The losses can be attributed to the plasmonic propagation losses of 5 dB in the 9 μm long slot, to the fiber-to-slot couplers with 4.5 dB per coupler and to extra insertion losses in the optical fiber array in order of 1 dB. When implementing the single devices into an array, narrower slot widths were obtained. As a result, the 55 nm wide plasmonic slot waveguide losses increased to 7 dB. Also, fiber-to-slot coupling to the narrower plasmonic slot waveguide resulted in 6.5 dB loss per coupler. This way, fiber-to-fiber losses at 1550 nm amounted to 21.5 ± 0.5 dB – uniformly for all devices across the array – see Fig. 3(b).

B. Frequency Response

The frequency response of the individual modulators was measured by applying a sinusoidal signal to the plasmonic modulator and measuring the modulation strength in an optical spectrum analyzer (OSA), see Fig. 4. The electro-optical 1 dB bandwidth of the modulator including electrical lines and contact pads was found to exceed 70 GHz. This result is in good agreement with measurements performed on other devices over a larger frequency range up to 500 GHz [56]. Additionally, electro-optic modulation uniform across the array channels was obtained, see Fig. 3(c) for the case of modulating by a 100 GBd BPSK signal.

C. Electrical and Optical Crosstalk

For parallel operation of all four channels, both electrical and optical crosstalk should be minimal. Channel 3 (CH 3) was chosen as a reference for this investigation as it is centrally located.

Electrical crosstalk from adjacent channels might cause undesired electro-optic modulation in a central channel. The electrical crosstalk into CH 3 was measured by applying different electrical driving scenarios and analyzing the optical transmission spectrum measured with an OSA. As a reference, the spectrum of CH 3 (green) – when modulated by a 100 GBd non-return-to-zero binary phase shift keying signal – is given in Fig. 3(d). Then, electrical crosstalk was measured by turning off the electrical signal in CH 3 and turning it on in channel 2 (CH 2) or channel 4 (CH 4), respectively. It can be seen that crosstalk from CH 2 leaks at a few resonance frequencies into CH 3. Electrical crosstalk from CH 4 leaks at around ±43 GHz into CH 3. We attribute these resonances to the particular arrangement of the electrical access lines, see Fig. 3(a). The higher crosstalk from CH 4 can be explained by an RF line passing between the two channels. The average crosstalk from CH 2 into CH 3 and from CH 4 into CH 3 amounts to −25 dB and −15 dB, respectively. The seeming increase in crosstalk for low frequencies (<5 GHz) stems from the filter bandwidth of the OSA in the measurement. A decrease in crosstalk towards 0 Hz is expected. Similar results were found when performing the electrical crosstalk experiments with other reference channels. In any case, the electrical crosstalk led to a signal modulation which was found to be below the amplified spontaneous emission (ASE) noise floor of low-noise erbium-doped fiber amplifiers (EDFA) in the receiver, see dashed line in Fig. 3(d). Therefore, we concluded a negligible induced SNR penalty. Also, from data experiments with simultaneous operation of multiple channel, it can be deduced that electrical crosstalk can at worst lead to a penalty of 0.5 dB, see Section VI.

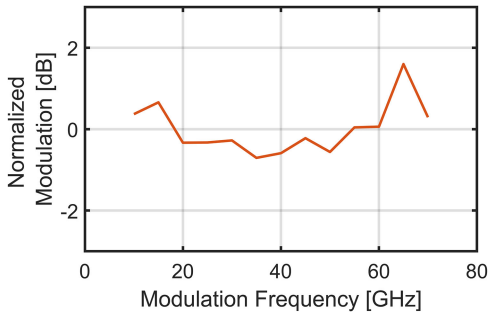

Fig. 4. The electro-optic response of the plasmonic modulators was measured by applying a sinusoidal signal and measuring the modulation strength with an OSA. The 1 dB bandwidth was found to exceed 70 GHz.

Optical crosstalk was measured accordingly. Electrically, all channels were turned off. Again CH 3 transmission (green) is given as a reference. Subsequently, optical input was changed to CH 2 or CH 4, respectively, while measuring transmission in CH 3. Optical crosstalk was measured to be −26.0 dB from CH 2 and −18.4 dB from CH 4, see Fig. 3(e). It is most likely caused by light scattered on-chip that strays into neighboring cores. The increased crosstalk from CH 4 is due to the proximity of its input core to CH 3 output core (c.f. Fig. 3(a)) while from CH 2 the output core is adjacent. The optical crosstalk led to a signal-to-noise ratio (SNR) penalty below 1.1 dB with respect to the single channel operation extracted from the array experiment shown below.

V. Single Channel Performance

The individual plasmonic interconnect channels were tested for high-speed data modulation with 100 GBd phase shift keying (PSK).

Data modulation experiments were carried out for each channel separately (c.f. array setup in Fig. 5). Electrically, 100 GBd non-return-to-zero (NRZ) signals were applied for binary phase shift keying (BPSK) and four level PSK (4-PSK). A signal with 650 mV voltage swing was generated with a digital-to-analog converter (DAC, Micram DAC4) and amplified to $V_p = 2.71$ V and $V_{rms} = 1.55$ V in case of BPSK and to $V_p = 2.36$ V and $V_{rms} = 0.93$ V in case of 4-PSK, respectively. The plasmonic modulators were contacted by an RF probe. For 4-PSK, a predistortion of the electrical signal was applied that mitigates the linear and nonlinear impairments of the driver electronics. Optically, a carrier at 1550 nm with an input power of 0.5 dBm for BPSK and 4.5 dBm for 4-PSK was fed into the fiber. In the receiver, the optical signal was amplified and band-pass filtered

TABLE I
SINGLE CHANNEL DATA TRANSMISSION EXPERIMENTS

PSK	BPSK				4-PSK			
Bitrate	100 Gbit/s				200 Gbit/s			
Channel	1	2	3	4	1	2	3	4
Eye Diagram	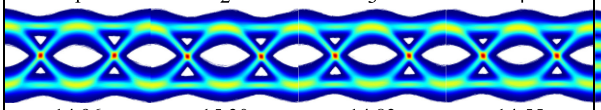				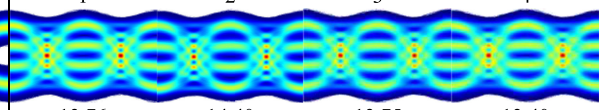			
SNR [dB]	14.96	15.30	14.83	14.55	13.76	14.40	13.75	13.40
BER	$< 10^{-5}$	$< 10^{-5}$	$< 10^{-5}$	$< 10^{-5}$	$1.25 \cdot 10^{-2}$	$0.84 \cdot 10^{-2}$	$1.23 \cdot 10^{-2}$	$1.50 \cdot 10^{-2}$

100 GBd single-channel data modulation experiment. The experiment was carried out at a wavelength of 1550 nm with optical input power of 0.5 dBm for BPSK or 4.5 dBm for 4-PSK. For BPSK, all four channels transmitted 100 Gbit/s with ~15 dB SNR and BERs below 10^{-5}. For 4-PSK, 200 Gbit/s per channel were demonstrated at SNR values around 14 dB and BERs below $1.50 \cdot 10^{-2}$. The SNR was determined from the distribution of the received and synchronized data.

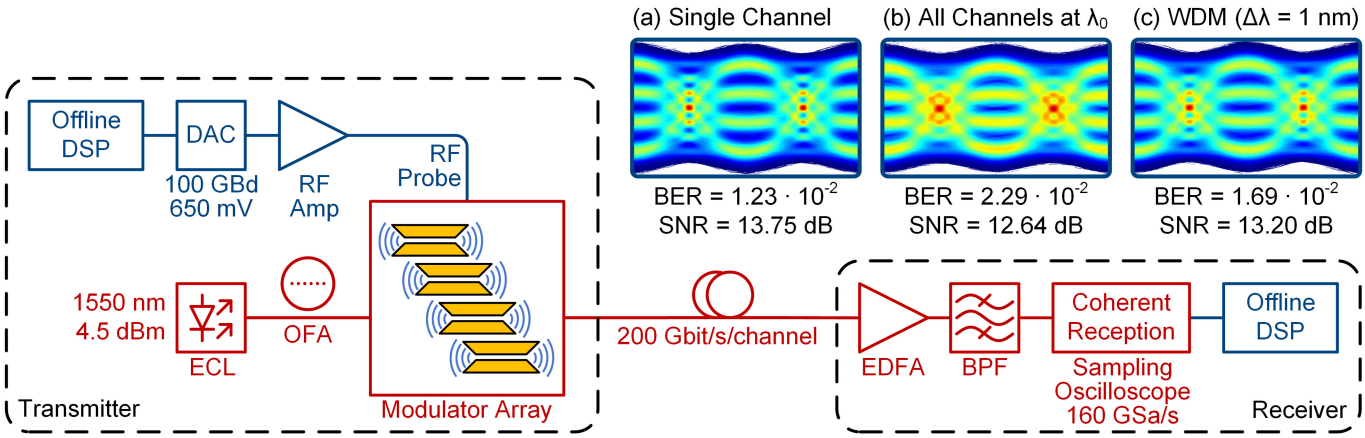

Fig. 5. Schematic of the experimental setup used for the array demonstration. At the transmitter, independent 100 GBd electrical signals are amplified and simultaneously driving the plasmonic modulators in the array. A 12 μm pitch optical fiber array (OFA) is used to couple the optical carriers at $\lambda_0 = 1550$ nm into and out of the plasmonic modulators. At the receiver, the optical signal is amplified in a EDFA and band-pass filtered (BPF) before being detected with a coherent reception scheme. Offline DSP is applied for signal recovery and equalization. The insets show the eye diagrams of channel 3 under varying conditions. (a) Other channels turned off. (b) All channels running at the same wavelength λ_0 to mimic a SDM scheme. The BER remained below the SD-FEC limit for 200 Gbit/s 4-PSK. An SNR penalty of 1.1 dB was found with respect to the single channel reference experiment from (a). (c) Neighboring channels have different wavelengths (1 nm wavelength spacing). This mimics a WDM-SDM scenario. The single channel performance is almost retained (SNR penalty of 0.5 dB).

before being coherently detected. In an offline DSP block, the frequency, phase and timing errors were corrected and linear equalization was applied to retrieve the transmitted data. All devices achieved data modulation of 100 Gbit/s below the KP4 forward error correction (FEC) limit [63] and 200 Gbit/s below the soft-decision (SD) FEC limit [64], respectively.

Table I compares the four array channels. The bit error ratio (BER) for BPSK was below 10^{-5} for all channels and for 4-PSK in the range between $0.8 \cdot 10^{-2}$ and $1.5 \cdot 10^{-2}$. Very consistent performance across all channels was demonstrated, which shows reproducibility and makes plasmonic modulator arrays a viable option for large-scale ultra-dense parallelization.

VI. PLASMONIC ARRAY INTERCONNECT EXPERIMENT

Parallel operation of the plasmonic array interconnect at 200 Gbit/s per channel was demonstrated with the experimental setup shown in Fig. 5. A multi-channel RF probe and a fiber array were used to operate three channels simultaneously (limited to three by our experimental equipment). Electrical signals built from randomly generated bits were driving the modulators. As an optical source, light from continuous wave lasers operated at telecom wavelength of 1550 nm with 4.5 dBm optical input power was launched into the fiber. After modulation, all channels were coupled back to the fiber array and fed to the receiver, where the signal was amplified, filtered and detected in a coherent homodyne detection scheme. While direct or differential detection is often preferred for simplicity and low cost, coherent detection was used as a proof of concept. In an offline digital signal processing (DSP) step, signal recovery and equalization were performed to retrieve the sent signal.

100 GBd data modulation experiments were carried out in two different scenarios. In a first scenario, the array was operated at a single wavelength to mimic space division multiplexing (SDM) with the cores of an optical fiber array. In a second scenario, the modulators in the array were operated with laser sources spaced by 1 nm. Hence, the latter corresponds to a combination of SDM and wavelength division multiplexing (WDM). It is expected that this scenario is less prone to optical crosstalk. In both scenarios, 100 Gbit/s BPSK and 200 Gbit/s 4-PSK were modulated and BERs below the KP4- and the SD-FEC limit were found, respectively. Again, the central channel (CH 3) was chosen as reference for the investigation. Fig. 5 inset (a) shows its single channel performance for comparison.

Space division multiplexing (SDM) is the most straightforward application of the suggested high-density transmitter as it minimizes additional system complexity. An operation wavelength λ_0 of 1550 nm was used for all channels. For 100 GBd BPSK, a bit error ratio (BER) below 10^{-5} and an SNR of 14 dB were measured in the central channel 3. For 100 GBd 4-PSK, the measured BER was $2.29 \cdot 10^{-2}$ with an SNR of 12.64 dB, see eye diagram in inset (b) of Fig. 5. Since electrical crosstalk was found to be minimal, the SNR penalty of 1.1 dB is mainly attributed to optical crosstalk. Nevertheless, the data experiment shows that crosstalk is no limiting factor.

Wavelength division multiplexing (WDM) can be combined with SDM as a further application scenario for such densely integrated interconnects. Potentially, all channels can be combined in a single fiber link between transmitter and receiver. To mimic such a scenario, the array channels were operated with a wavelength spacing $\Delta\lambda$ of 1 nm. 200 Gbit/s were transmitted with a BER of $1.69 \cdot 10^{-2}$ and an SNR of 13.2 dB. The corresponding eye diagram is shown in Fig. 5 inset (c). The reduced optical crosstalk allowed almost single channel performance.

In summary, we demonstrated a plasmonic array interconnect with 4×200 Gbit/s data modulation, operational mimicking pure SDM or its combination with WDM.

VII. Conclusion

This work demonstrates extremely dense integration of four plasmonic modulator channels for optical interconnects. 0.8 Tbit/s were modulated on an area of only 90 µm × 5.5 µm. Operation in space and wavelength division multiplexing was demonstrated without degeneration of the transmitted data rates. Hence, the presented transmitter renders a flexible component for high-speed interconnects. Furthermore, such a compact device concept enables new options for dense co-integration with electronics.

References

[1] D. A. B. Miller, "Physical reasons for optical interconnection," *Int. J. Optoelectron.*, vol. 11, no. 3, pp. 155–168, May/Jun. 1997.

[2] Z. H. Li, I. Shubin, and X. Zhou, "Optical interconnects: Recent advances and future challenges," *Opt. Express*, vol. 23, no. 3, pp. 3717–3720, Feb. 5, 2015.

[3] D. A. B. Miller, "Attojoule optoelectronics for low-energy information processing and communications," *J. Lightw. Technol.*, vol. 35, no. 3, pp. 346–396, Jan. 3, 2017.

[4] P. J. Winzer and D. T. Neilson, "From scaling disparities to integrated parallelism: A decathlon for a decade," *J. Lightw. Technol.*, vol. 35, no. 5, pp. 1099–1115, Feb. 1, 2017.

[5] X. Zhou, H. Liu, and R. Urata, "Datacenter optics: Requirements, technologies, and trends," *Chin. Opt. Lett.*, vol. 15, no. 5, pp. 120008-1–120008-4, Mar. 17, 2017.

[6] C. A. Thraskias *et al.*, "Survey of photonic and plasmonic interconnect technologies for intra-datacenter and high-performance computing communications," *IEEE Commun. Surv. Tut.*, vol. 20, no. 4, pp. 2758–2783, May 28, 2018.

[7] A. V. Krishnamoorthy *et al.*, "Computer systems based on silicon photonic interconnects," *Proc. IEEE*, vol. 97, no. 7, pp. 1337–1361, Jun. 10, 2009.

[8] A. V. Krishnamoorthy *et al.*, "From chip to cloud: Optical interconnects in engineered systems," *J. Lightw. Technol.*, vol. 35, no. 15, pp. 3103–3115, Dec. 20, 2016.

[9] C. Minkenberg *et al.*, "Reimagining datacenter topologies with integrated silicon photonics," *J. Opt. Commun. Netw.*, vol. 10, no. 7, pp. B126–B139, Jul. 13, 2018.

[10] H. Ito, S. Kodama, Y. Muramoto, T. Furuta, T. Nagatsuma, and T. Ishibashi, "High-speed and high-output InP-InGaAs unitraveling-carrier photodiodes," *IEEE J. Sel. Topics Quantum Electron.*, vol. 10, no. 4, pp. 709–727, Oct. 18, 2004.

[11] L. Vivien *et al.*, "Zero-bias 40 Gbit/s germanium waveguide photodetector on silicon," *Opt. Express*, vol. 20, no. 2, pp. 1096–1101, Jan. 4, 2012.

[12] H. T. Chen *et al.*, "100-Gbps RZ data reception in 67-GHz Si-contacted germanium waveguide p-i-n photodetectors," *J. Lightw. Technol.*, vol. 35, no. 4, pp. 722–726, Jul 21, 2016.

[13] Y. Salamin *et al.*, "100 GHz plasmonic photodetector," *ACS Photon.*, vol. 5, no. 8, pp. 3291–3297, Jun. 24, 2018.

[14] P. Runge *et al.*, "Waveguide integrated balanced photodetectors for coherent receivers," *IEEE J. Sel. Topics Quantum Electron.*, vol. 24, no. 2, Jul 5, 2018, Art. no. 6100307.

[15] Y. Ding *et al.*, "Ultra-compact graphene plasmonic photodetector with the bandwidth over 110 GHz," Aug. 13, 2018. arXiv: 1808.04815v2.

[16] P. Ma *et al.*, "Plasmonically enhanced graphene photodetector featuring 100 Gbit/s data reception, high-responsivity and compact size," *ACS Photon.*, vol. 6, no. 1, pp. 154–161, Nov. 29, 2018.

[17] L. Chen, C. R. Doerr, L. Buhl, Y. Baeyens, and R. A. Aroca, "Monolithically integrated 40-wavelength demultiplexer and photodetector array on silicon," *IEEE Photon. Technol. Lett.*, vol. 23, no. 13, pp. 869–871, Apr. 7, 2011.

[18] T. J. Seok, V. Kopp, D. Neugroschl, J. Henriksson, J. H. Luo, and M. C. Wu, "High density optical packaging of high radix silicon photonic switches," in *Proc. Opt. Fiber Commun. Conf. Exhib.*, Mar. 2017, pp. 1–3.

[19] D. J. Richardson, J. M. Fini, and L. E. Nelson, "Space-division multiplexing in optical fibres," *Nature Photon.*, vol. 7, no. 5, pp. 354–362, Apr. 29, 2013.

[20] K. Saitoh and S. Matsuo, "Multicore fiber technology," *J. Lightw. Technol.*, vol. 34, no. 1, pp. 55–66, Aug. 20, 2015.

[21] R. S. Luís *et al.*, "1.2 Pb/s transmission over a 160 µm cladding, 4-core, 3-mode fiber, using 368 C+L band PDM-256-QAM channels," in *Proc. Eur. Conf. Opt. Commun.*, Sep. 2018, pp. 1–3.

[22] S. Berdague and P. Facq, "Mode division multiplexing in optical fibers," *Appl. Opt.*, vol. 21, no. 11, pp. 1950–1955, Jun. 1, 1982.

[23] C. R. Doerr, N. K. Fontaine, M. Hirano, T. Sasaki, L. L. Buhl, and P. J. Winzer, "Silicon photonic integrated circuit for coupling to a ring-core multimode fiber for space-division multiplexing," in *Proc. Eur. Conf. Opt. Commun.*, Sep. 2011, pp. 1–3.

[24] N. Bozinovic *et al.*, "Terabit-scale orbital angular momentum mode division multiplexing in fibers," *Science*, vol. 340, no. 6140, pp. 1545–1548, Jun. 28, 2013.

[25] R. Ryf *et al.*, "High-spectral-efficiency mode-multiplexed transmission over graded-index multimode fiber," in *Proc. Eur. Conf. Opt. Commun.*, Sep. 2018, pp. 1–3.

[26] F. E. Doany *et al.*, "160 Gb/s bidirectional polymer-waveguide board-level optical interconnects using CMOS-based transceivers," *IEEE Trans. Adv. Packag.*, vol. 32, no. 2, pp. 345–359, May 15, 2009.

[27] Y. Wang *et al.*, "A high-speed 84 Gb/s VSB-PAM8 VCSEL transmitter-based fiber–IVLLC integration," *IEEE Photon. J.*, vol. 10, no. 5, pp. 1–8, Sep. 3, 2018.

[28] P. Westbergh, J. S. Gustavsson, and A. Larsson, "VCSEL arrays for multicore fiber interconnects with an aggregate capacity of 240 Gb/s," *IEEE Phot. Technol. Lett.*, vol. 27, no. 3, pp. 296–299, Nov. 12, 2014.

[29] A. Larsson, P. Westbergh, J. S. Gustavsson, E. Haglund, and E. P. Haglund, "High speed VCSELs and VCSEL arrays for single and multicore fiber interconnects," *Proc. SPIE*, vol. 9381, Mar. 4, 2015, Art. no. 93810D.

[30] J. Van Kerrebrouck *et al.*, "High-speed PAM4-based optical SDM interconnects with directly modulated long-wavelength VCSEL," *J. Lightw. Technol.*, p. 1, Oct. 11, 2018.

[31] C. Wang, M. Zhang, B. Stern, M. Lipson, and M. Loncar, "Nanophotonic lithium niobate electro-optic modulators," *Opt. Express*, vol. 26, no. 2, pp. 1547–1555, Jan. 16, 2018.

[32] X. Chen *et al.*, "Generation and intradyne detection of single-wavelength 1.61-Tb/s using an all-electronic digital band interleaved transmitter," in *Proc. Opt. Fiber Commun. Conf. Expo.*, Mar. 2018, pp. 1–3.

[33] C. Wang *et al.*, "Integrated lithium niobate electro-optic modulators operating at CMOS-compatible voltages," *Nature*, vol. 562, no. 7725, pp. 101–104, Oct. 4, 2018.

[34] R. Nagarajan *et al.*, "InP photonic integrated circuits," *IEEE J. Sel. Topics Quantum Electron.*, vol. 16, no. 5, pp. 1113–1125, Jan. 26, 2010.

[35] V. Katopodis *et al.*, "Serial 100 Gb/s connectivity based on polymer photonics and InP-DHBT electronics," *Opt. Express*, vol. 20, no. 27, pp. 28538–28543, Dec. 10, 2012.

[36] Y. Ogiso *et al.*, "Over 67 GHz bandwidth and 1.5 V Vπ InP-based optical IQ modulator with n-i-p-n heterostructure," *J. Lightw. Technol.*, vol. 35, no. 8, pp. 1450–1455, Dec. 13, 2016.
[37] O. Ozolins *et al.*, "100 GHz externally modulated laser for optical interconnects," *J. Lightw. Technol.*, vol. 35, no. 6, pp. 1174–1179, Jan. 10, 2017.
[38] S. Lange *et al.*, "100 GBd intensity modulation and direct detection with an InP-based monolithic DFB laser Mach-Zehnder modulator," *J. Lightw. Technol.*, vol. 36, no. 1, pp. 97–102, Aug. 22, 2017.
[39] H. Mardoyan *et al.*, "204-GBaud on-off keying transmitter for inter-data center communications," in *Proc. Opt. Fiber Commun. Conf. Expo.*, San Diego, CA, USA, Mar. 2018, Paper Th4A.4.
[40] S. Arafin and L. A. Coldren, "Advanced InP photonic integrated circuits for communication and sensing," *IEEE J. Sel. Topics Quantum Electron.*, vol. 24, no. 1, pp. 1–12, Sep. 20, 2018.
[41] R. Going *et al.*, "4 $\times$ 600 Gb/s photonic IC transmitter and receiver modules," in *Proc. Eur. Conf. Opt. Commun.*, Sep. 2018, pp. 1–3.
[42] H. Yamazaki *et al.*, "Transmission of 400-gbps discrete multi-tone signal using $>$100-GHz-bandwidth analog multiplexer and InP Mach-Zehnder modulator," in *Proc. Eur. Conf. Opt. Commun.*, Sep. 2018, pp. 1–3.
[43] J. Leuthold *et al.*, "Silicon-organic hybrid electro-optical devices," *IEEE J. Sel. Topics Quantum Electron.*, vol. 19, no. 6, Aug. 15, 2013, Art. no. 3401413.
[44] J. Verbist *et al.*, "Real-time 100 Gb/s NRZ and EDB transmission with a GeSi electroabsorption modulator for short-reach optical interconnects," *J. Lightw. Technol.*, vol. 36, no. 1, pp. 90–96, Nov. 19, 2017.
[45] S. Wolf *et al.*, "Coherent modulation up to 100 GBd 16QAM using silicon-organic hybrid (SOH) devices," *Opt. Express*, vol. 26, no. 1, pp. 220–232, Jan. 3, 2018.
[46] J. C. Lin, H. Sepehrian, L. A. Rusch, and W. Shi, "CMOS-compatible silicon photonic IQ modulator for 84 gbaud 16QAM and 70 Gbaud 32QAM," in *Proc. Opt. Fiber Commun. Conf. Expo.*, Mar. 2018, pp. 1–3.
[47] J. Sun, R. Kumar, M. Sakib, J. Driscoll, H. Jayatilleka, and H. Rong, "A 128 Gb/s PAM4 silicon microring modulator with integrated thermo-optic resonance tuning," *J. Lightw. Technol.*, vol. 37, no. 1, pp. 110–115, Jan. 2019.
[48] A. Emboras *et al.*, "Electrically controlled plasmonic switches and modulators," *IEEE J. Sel. Topics Quantum Electron.*, vol. 21, no. 4, Dec. 18, 2014, Art. no. 4600408.
[49] C. Haffner *et al.*, "Plasmonic organic hybrid modulators-scaling highest speed photonics to the microscale," *Proc. IEEE*, vol. 104, no. 12, pp. 2362–2379, Jun. 7, 2016.
[50] C. Hoessbacher *et al.*, "Plasmonic modulator with $>$170 GHz bandwidth demonstrated at 100 GBd NRZ," *Opt. Express*, vol. 25, no. 3, pp. 1762–1768, Jan. 23, 2017.
[51] A. Messner *et al.*, "Plasmonic ferroelectric modulators," *J. Lightw. Technol.*, p. 1, Nov. 14, 2018.
[52] W. Heni *et al.*, "Plasmonic IQ-modulators with attojoule per bit electrical energy consumption," to be published.
[53] E. Timurdogan, C. M. Sorace-Agaskar, J. Sun, E. S. Hosseini, A. Biberman, and M. R. Watts, "An ultralow power athermal silicon modulator," *Nature Commun.*, vol. 5, Jun. 11, 2014, Art. no. 4008.
[54] C. Haffner *et al.*, "Low-loss plasmon-assisted electro-optic modulator," *Nature*, vol. 556, no. 7702, pp. 483–486, Apr. 25, 2018.
[55] B. Baeuerle *et al.*, "Reduced equalization needs of 100 GHz bandwidth plasmonic modulators," to be published.
[56] M. Burla *et al.*, "500 GHz plasmonic Mach-Zehnder modulator enabling sub-THz microwave photonics," to be published.
[57] I. C. Benea-Chelmus *et al.*, "Three-dimensional phase modulator at telecom wavelength acting as a terahertz detector with an electro-optic bandwidth of 1.25 terahertz," *ACS Photon.*, vol. 5, no. 4, pp. 1398–1403, Feb. 21, 2018.
[58] W. Heni *et al.*, "High speed plasmonic modulator array enabling dense optical interconnect solutions," *Opt. Express*, vol. 23, no. 23, pp. 29746–29757, Nov. 5, 2015.
[59] M. Ayata *et al.*, "High-speed plasmonic modulator in a single metal layer," *Science*, vol. 358, no. 6363, pp. 630–632, Nov. 3, 2017.
[60] M. Ayata *et al.*, "All-plasmonic IQ modulator with 36 um fiber-to-fiber pitch," in *Proc. Eur. Conf. Opt. Commun.*, Sep. 2018, pp. 1–3.
[61] U. Koch *et al.*, "Ultra-compact 0.8 Tbit/s plasmonic modulator array," in *Proc. Eur. Conf. Opt. Commun.*, Sep. 2018, pp. 1–3.
[62] D. L. Elder *et al.*, "Effect of rigid bridge-protection units, quadrupolar interactions, and blending in organic electro-optic chromophores," *Chem. Mater.*, vol. 29, no. 15, pp. 6457–6471, Jul. 7, 2017.
[63] E. El-Fiky *et al.*, "First demonstration of a 400 Gb/s 4 lambda CWDM TOSA for datacenter optical interconnects," *Opt. Express*, vol. 26, no. 16, pp. 19742–19749, Jul. 23, 2018.
[64] K. Schuh *et al.*, "Single carrier 1.2 Tbit/s transmission over 300 km with PM-64 QAM at 100 GBaud," in *Proc. Opt. Fiber Commun. Conf. Expo.*, Mar. 2017, pp. 1–3.

Ueli Koch received the M.Sc. degree in computational science and engineering from ETH Zurich, Zurich, Switzerland, in 2013. He is currently working toward the Ph.D. degree in the Institute of Electromagnetic Fields at ETH Zurich. His current research interests include the numerical modeling and simulation of surface effects in plasmonic nanostructures with a particular focus on electro-optic modulation.

Andreas Messner received the B.Sc. and M.Sc. degrees in electrical engineering and information technology from the Karlsruhe Institute of Technology (KIT), Karlsruhe, Germany, in 2013 and 2015, respectively. Since 2015, he has been working toward the Ph.D. degree in the group of Prof. J. Leuthold at ETH Zurich, Zurich, Switzerland.

From 2010 to 2015, he investigated and modeled battery and fuel cell electrode materials as a Student Research Assistant with the Institute of Materials for Electrical and Electronic Engineering, Karlsruhe Institute of Technology. From December 2013 to May 2014, he was part of the network infrastructure group in the Guiana Space Centre, Kourou, France. Today, his research interests comprise integrated photonics and plasmonics and their combination with nonlinear optical materials.

Claudia Hoessbacher received the B.Sc. degree in electrical engineering and information technology and the M.Sc. degree in optics and photonics from Karlsruhe Institute of Technology, Karlsruhe, Germany in 2010 and 2012, respectively, and the Dr.sc. degree (Ph.D.) from ETH Zurich, Zurich, Switzerland, in 2017. Her research interests include design, fabrication and testing of integrated photonics, plasmonics, and high-speed electro-optics.

Wolfgang Heni received the M.Sc. degree in electrical engineering and information technology from the Karlsruhe Institute of Technology, Karlsruhe, Germany, in 2013. He is currently working toward the Ph.D. degree in electrical engineering at ETH Zurich, Zurich, Switzerland, in the group of Prof. J. Leuthold. From April 2012 to September 2012, he visited the Photonics System Group, Tyndall National Institute, Cork, Ireland, U.K., as a research intern. His research focuses on the in-device optimization and the application of nonlinear optical materials, integrated photonics, plasmonics, and electro-optical devices.

Arne Josten was born in Germany, in 1986. He received the M.Sc. degree in electrical engineering and information technology from the Karlsruhe Institute of Technology (KIT), Karlsruhe, Germany, in 2013. He is currently working toward the Ph.D. degree at ETH Zurich, Zurich, Switzerland, in the group of Prof. Juerg Leuthold. His research interests are digital signal processing for high-speed optical communication and the real-time capability of the developed schemes.

Benedikt Baeuerle was born in Germany, in 1987. He received the B.Sc. and M.Sc. degrees in electrical engineering and information technology from the Karlsruhe Institute of Technology (KIT), Karlsruhe, Germany, in 2010 and 2013, respectively. He is currently working toward the Ph.D. degree at Institute of Electromagnetic Fields (IEF), ETH Zurich, Zurich, Switzerland. From March 2012 to August 2012, he visited the Photonics System Group, Tyndall National Institute, Cork, Ireland, U.K., as a research intern. His research interests include digital signal processing, real-time processing, digital coherent transceivers, and optical transmission systems and subsystems.

Masafumi Ayata was born in Japan, in 1990. He received the B.Sc. and M.Sc. degrees in electrical engineering and information systems from the University of Tokyo, Tokyo, Japan, in 2013 and 2015, respectively. He is currently working toward the Ph.D. degree at the Institute of Electromagnetic Fields, ETH Zurich, Zurich, Switzerland. His research interests include photonic integrated circuits, integrated plasmonic devices, and optical communications.

Yuriy Fedoryshyn received the Master's degree in laser and optoelectronic technology from Lviv Polytechnic National University, Lviv, Ukraine, and the Ph.D. degree in electrical engineering from ETH Zurich, Zurich, Switzerland. He is currently leading the micro- and nanofabrication activities with the Institute of Electromagnetic Fields, ETH Zurich. His research interests include plasmonic and nanophotonic devices, including modulators, switches, detectors, and light sources.

Delwin L. Elder received the B.S. degree in chemistry from the University of North Carolina, Chapel Hill, NC, USA, in 1994, and the Ph.D. degree from the California Institute of Technology, Pasadena, CA, USA, in 1999. From 1999 to 2009, he was a Senior Research Chemist with the Air Products and Chemicals, Inc. (now Evonik), where his research and development projects included polymer electrolytes for lithium batteries and charge transport conducting polymers, among other things. Since 2010, he has been a Research Scientist and Lab Manager with the Chemistry Department, University of Washington, Seattle, WA, USA. His research interests include design and synthesis of organic nonlinear optical chromophores, thin film device fabrication, and measurement of electro-optic coefficients, spectroscopic and physical properties, and bulk molecular order.

Larry R. Dalton (SM'06) received the B.S. and M.S. degrees from the Honors College of Michigan State University, East Lansing, MI, USA, in 1965 and 1966, respectively, and the A.M. and Ph.D. degrees from Harvard University, Cambridge, MA, USA, in 1971. He has held appointments in chemistry, electrical engineering, chemical engineering, and biochemistry, including the B. Seymour Rabinovitch Chair (University of Washington), the George B. Kauffman Professorship (UW), and the Harold and Lillian Moulton Chair (University of Southern California). He has directed or codirected the Loker Hydrocarbon Research Institute (USC), the National Science Foundation Science and Technology Center on Materials and Devices for Information Technology Research, the DARPA MORPH Program, and two DoD MURI Centers. He has coauthored more than 700 publications and patents. He is currently a Presidential Laureate of the University of Washington, Seattle, WA, USA, and is the Chair of the Washington State Academy of Science Working Group on Environmental Quality, Sustainability, and Climate Change.

Dr. Dalton was elected as a Fellow of OSA, ACS, MRS, SPIE, and AAAS. His recent awards include a SPIE Lifetime Achievement Award, the IEEE/LEOS William Streifer Award, the American Chemical Society Award in the Chemistry of Materials, the ACS Linus Pauling Award and Medal, the ACS Richard C. Tolman Medal, and a Helmholtz International Fellow Award. He has been honored with a Festschrift Issue of the *ACS Journal of Physical Chemistry*.

Juerg Leuthold (F'13) received the Ph.D. degree in physics from ETH Zurich, Zurich, Switzerland, for work in the field of integrated optics and all-optical communications, in 1998. Since 2013, he has been the head of the Institute of Electromagnetic Fields (IEF), ETH Zurich, Zurich, Switzerland. From 2004 to 2013, he was affiliated with the Karlsruhe Institute of Technology, Karlsruhe, Germany, where he was the Head of the Institute of Photonics and Quantum Electronics and the Helmholtz Institute of Microtechnology. From 1999 to 2004, he was affiliated with Bell Labs, Lucent Technologies, Holmdel, NJ, USA, where he performed device and system research with III/V semiconductor and silicon optical bench materials for applications in high-speed telecommunications. His interests are in the field of photonics, plasmonics, and microwave with an emphasis on applications in communications and sensing.

Dr. Leuthold is a fellow of the Optical Society of America (OSA) and a member of the Heidelberg Academy of Science. He served the community as a member of the Helmholtz Association Think Tank, as a member of the board of directors of OSA, and in many technical program committees or as the general chair of meetings.